Available online at www.sciencedirect.com
ScienceDirect
Coordination Chemistry Reviews 252 (2008) 1079–1092
COORDINATION CHEMISTRY REVIEWS
www.elsevier.com/locate/ccr

Review

Supramolecular edifices and switches based on metals

Mourad Elhabiri, Anne-Marie Albrecht-Gary *

Laboratoire de Physico-Chimie Bioinorganique, ULP-CNRS (UMR 7177), Institut de Chimie, ECPM, 25 rue Becquerel, 67200 Strasbourg, France

Received 1 June 2007; accepted 17 September 2007
Available online 21 September 2007

Contents

Abstract

Our studies allowed to unravel at least partially, the "so-called" spontaneous self-assembly processes of supramolecular edifices based on metals. The formation of a tricuprous double-stranded helix in solution was found to be driven by thermodynamics via highly distorted intermediates. Dinuclear europium(III) triple-stranded helices were built in solution via alternative "braiding" and "keystone" mechanism. The overall process was also dominated by thermodynamics. Moreover, multipodal ligand with the appropriate binding sites can operate as Cu(II)/Cu(I) molecular switches. Recently, we examined ligands with neighboring binding functionalities (*N*,*N*) and (*N*,*O*) which confer to the corresponding divalent metal complexes new properties. They could operate as proton-driven multistage molecular switching devices based on region-selective metal binding.

Keywords: Europium; Copper; Iron; Helicates; Redox- and pH-driven molecular switch; Bipod; Supramolecular complexes; Nanomaterials; Self-assembly mechanisms

1. Introduction

Harmonizing the functionalities of individual moieties in a supramolecular arrangement [1] represents a versatile approach for developing well-defined architectures with pre-programmed conformations and pre-determined magnetic, electronic, photophysical and/or physico-chemical properties [2]. Among the large panoply of non-covalent interactions [3] used to induce this hierarchical organization, metal-directed supramolecular self-assembly [4,5] has proven to be a powerful mean to construct stable nanoscale edifices, which are beginning to approach the necessary degree of complexity to serve as useful and functional molecular machines. [6] Nevertheless, it is generally accepted that one cannot accurately predict the spontaneously organized structures by simple design or from physical principles. The self-assembly of metal-organic frameworks is indeed highly influenced by various exogenous factors such as solvent, temperature, pH, counter-ions as well as intrinsic parameters such as geometric requirements, charges and solvation of the metal ion and conformational variation, rigidity/flexibility balance, number and nature of the binding sites and charges of the organic backbones [1]. Therefore, much more fundamental work

* Corresponding author. Tel.: +33 390 24 26 38; fax: +33 390 24 26 39.
E-mail address: amalbre@chimie.u-strasbg.fr (A.-M. Albrecht-Gary).

0010-8545/$ – see front matter © 2007 Published by Elsevier B.V.
doi:10.1016/j.ccr.2007.09.014

is essential to broaden our knowledge of the relevant structural types, and a good understanding of self-assembly mechanisms of supramolecules and dynamics of molecular machines will consequently allow chemists to master the design of ingenious systems, leading to valuable supramolecular precursors for functional devices.

Various helicates have been reported so far [5,7,8], and they are essentially characterized by their molecular structure and, sometimes, by their thermodynamic parameters. Kinetic data, which are essential for deciphering the self-assembly mechanism and, therefore, for understanding the recognition process, are extremely scarce. We will first address herein some of the questions in relation to self-assembly processes through relevant examples of double- and triple-stranded helicates.

The field of molecular-electronics requests such individual nanoscale supramolecular precursors to execute functions in electronic circuitry currently performed by semiconductor devices. This emerging field is evolving rapidly with the envisioned perspectives to overcome the foreseen physical limits of conventional microelectronics [9]. Even though there are no commercial applications as yet, the scientific contributions coming out of this extensive research are spectacular [10], and the potential applications are almost endless. In this molecular-electronics research, supramolecules are used to mimic the active and passive components (switches, memory circuits, rectifiers, logic gates, sensors, diodes, resistors and LEDs) of electronic or integrated circuits. Progress toward incorporating such objects in electronic circuitry has advanced rapidly over the past 5 years. Very recently, a 64-bit random access memory circuit using bistate rotaxanes as the memory elements was reported, and allowed to produce a 16-Kbit memory circuit at a density of devices that far exceeds current technology [11]. As part of this advance, the development of new molecular switches [12,13] and logical gates [14–16] remains an intricate challenge for supramolecular chemists [1].

A multistate molecular switch is defined as any molecule or supramolecular ensemble, which can be found in two or more stable states with distinctly different properties, and in which the interconversion between the different states is possible through a simple and external triggering stimulus (photon, electron and ion). Such devices should operate with efficiency, reversibility and resistance to fatigue [1]. Among the numerous molecular switches reported in the literature, nanoscale molecular machines [6] are of fundamental interest, yielding dynamic edifices for which directionally motions can be easily induced and controlled.

A molecular machine is an edifice made of at least two components, one of which can be put in motion with respect to the other by an external signal [17]. Mechanical switching processes therefore consist of the reversible conversion of a multistable entity between two (or more) structurally and/or conformationally different states. These assemblies must be also controllable, reversible and readable at the molecular level. Supramolecular devices capable of performing such tasks are important building blocks that would play an outstanding role in the nanotechnological revolution of the twenty-first century.

This review is focused on the characterization of thermodynamic and kinetic intermediates leading to the targeted supramolecular edifices. Examples of self-assembling mechanisms in solution of polytopic strands and metals are presented. Combining the most recent development of analytical methods, intramolecular motion of cations, triggered by oxidation–reduction or by change of pH, are also examined in this article.

2. Deciphering the self-assembly mechanisms of metallohelicates

Metal-based supramolecules have thus attracted attention in the last decades [1]. For example, designing helicates containing two or more ions in close proximity is of great interest for decreasing negative intramolecular interactions, and so gathering in close proximity spectroscopic, spectrophotometric or magnetic probes [8]. It is also of importance to investigate meticulously the physicochemical characteristics of helicate formation in solution, which is very often reported as spontaneous and "magic".

2.1. Triple-stranded diferrous helicate

Ferrous complexes were studied as templates of metalloenzymes functions [18], of redox switches [19]. Diferrous double or tripodal helical complexes were examined by electrochemistry [20,21]. In collaboration with Pierre's group, we characterized by mass spectrometry and spectrophotometry the ferrous species, which are involved in the self-assembly process of a triple-stranded dinuclear helicate [22] with a flexible bis(2-2′-bipyridine) ligand $\mathbf{L^a}$ (Fig. 1).

Spectrophotometric titrations of free ligand $\mathbf{L^a}$ *versus* p[H] led to a model with three absorbing acid–base species:

$$\mathbf{L^a} + H^+ \overset{K_1}{\rightleftarrows} \mathbf{L^a}H^+ \quad (1)$$

$$\mathbf{L^a}H^+ + H^+ \overset{K_2}{\rightleftarrows} \mathbf{L^a}H_2{}^{2+} \quad (2)$$

with $\log K_1 = 4.54(4)$ and $\log K_2 = 3.6(1)$ in methanol. The successive protonations of $\mathbf{L^a}$ induce a bathochromic shift (10–20 nm) of the absorption band centered at 291 nm. A model involving three ferrous species, $\mathbf{L^a}_2Fe^{2+}$, $\mathbf{L^a}_2Fe^{4+}$ and $\mathbf{L^a}_3Fe_2{}^{4+}$, in agreement with ESMS spectra, was fitted using absorption spectrophotometry. The logarithmic values of the corresponding stability constants are, respectively equal to $\log \beta_1^{Fe} = 12.1(3)$, $\log \beta_2^{Fe} = 18.6(2)$ and $\log \beta_3^{Fe} = 25.50(6)$ in methanol.

$$2\mathbf{L^a} + Fe^{2+} \overset{\beta_1^{Fe}}{\rightleftarrows} \mathbf{L^a}_2Fe^{2+} \quad (3)$$

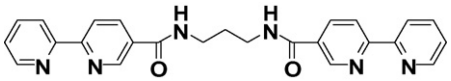

Fig. 1. Chemical formula of bis(2,2′-bipyridine) ligand $\mathbf{L^a}$.

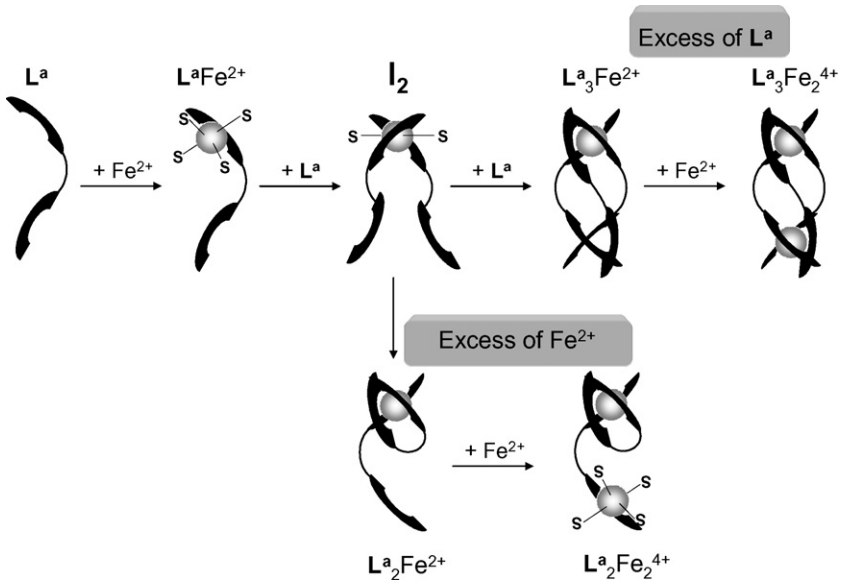

Fig. 2. Self-assembling process for the formation of the diferrous triple-stranded helicate; S = molecule of solvent; I_2 = intermediate.

$$2\mathbf{L^a} + 2Fe^{2+} \overset{\beta_2^{Fe}}{\rightleftarrows} \mathbf{L^a}_2Fe_2^{4+} \quad (4)$$

$$3\mathbf{L^a} + 2Fe^{2+} \overset{\beta_3^{Fe}}{\rightleftarrows} \mathbf{L^a}_3Fe_2^{4+} \quad (5)$$

The electronic spectra of monoferrous $\mathbf{L^a}_2Fe^{2+}$ and diferrous $\mathbf{L^a}_2Fe_2^{4+}$ complexes display a metal to ligand charge-transfer band centered at 540 nm. The intense absorption band at 500 nm [23,24], characteristic of tris(2,2′-bipyridine) ferrous complexes, was proven to be due to charge-transfer transitions from the 3d atomic orbital of iron(II) to the lowest vacant π molecular orbital of the ligand [25]. This band obscures d–d transitions of the metal, but can be distinguished from the π → π* transition bands of 2,2′-bipyridine at around 300 nm [26,27]. In high-spin octahedral iron(II) complexes, broad 5T2g → 5Eg transitions occur in the visible/near-IR region (900–1200 nm) [28]. The absorption spectra that we obtained for $\mathbf{L^a}_2Fe^{2+}$ and $\mathbf{L^a}_2Fe_2^{4+}$, then, clearly indicate the coordination of three 2,2′-bipyridine fragments. The only structure which can be proposed for $\mathbf{L^a}_2Fe^{2+}$ is the coordination of two 2,2′-bipyridine functions provided by a folded ligand $\mathbf{L^a}$, the third 2,2′-bipyridine coordination site being brought by a second extended strand $\mathbf{L^a}$ (Fig. 2). From $\mathbf{L^a}_2Fe^{2+}$ to $\mathbf{L^a}_2Fe_2^{4+}$, the addition of a second ferrous cation does not significantly affect the characteristic absorption band in the visible region of the low-spin $\mathbf{L^a}_2Fe^{2+}$ complex. This observation strongly suggests the coordination of the second ferrous cation on the free 2,2′-bipypridine moiety of the extended strand $\mathbf{L^a}$ in $\mathbf{L^a}_2Fe^{2+}$, since the formation of a mono(2,2′-bipyridine) high-spin ferrous complex cannot be detected in the visible region, but at longer wavelengths [28]. The structure that we propose for the thermodynamic $\mathbf{L^a}_2Fe^{2+}$ and $\mathbf{L^a}_2Fe_2^{4+}$ species agrees well with both the spectrophotometric data and the sequence of stability [31] observed for ferrous 2,2′-bipyridine complexes, since it does not imply the thermodynamic unfavorable ferrous species with two 2,2′-bipyridine coordination sites [29,31]. The helical structure of $\mathbf{L^a}_3Fe_2^{4+}$ was established by ^{1}H NMR [30] measurements.

The self-assembly mechanism of the diferrous triple-stranded helicate is driven by the drastic increase of stability of the low-spin tris-bipyridine complexes [31] compared to the labile high-spin mono- and bischelates (Fig. 2).

2.2. Double-stranded tricuprous helicate

The structure of double-stranded helicates based on multiple diimine binding sites and various transition metals have been well characterized by crystallography [5–33] and [5–34] NMR. Mass spectrometry was also used to confirm the stoichiometries of the corresponding supramolecules [35,36].

In collaboration with Lehn and his collaborators [37], we have investigated the nature of the species formed with copper(I) and an oligobipyridine strand $\mathbf{L^b}$ containing three 2,2′-bipyridine units separated by oxydimethylene bridges. Each bipyridine moiety is bearing two 4,4′-($CONEt_2$) substituents (Fig. 3).

Spectrophotometric titrations of $\mathbf{L^b}$ with copper(I) were carried out in order to calculate the binding constants of the complexes and to determine the corresponding electronic spectra (260–650 nm). The best fit of the spectrophotometric data was obtained by both Specfit [38–41] and Letagrop-Spefo [42–44] programs with a model including three complexes observed by ESMS, $\mathbf{L^b}Cu$, $\mathbf{L^b}_2Cu_2$ and $\mathbf{L^b}_2Cu_3$. The values of the corresponding stability constants are summarized in Table 1. The absorption spectra of the copper(I) complexes are dominated by

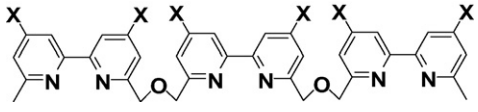

Fig. 3. Chemical structure of ligand $\mathbf{L^b}$ (X = $CONEt_2$).

Table 1
Global stability constants and spectrophotometric parameters for the cuprous complexes formed with $\mathbf{L^b}$ [a]

Equilibrium	$\log \beta$ (3σ)	λ_{max} (nm)	ε_{max} ($M^{-1}\,cm^{-1}$)
$\mathbf{L^b} + Cu \overset{\beta_{\mathbf{L^bCu}}}{\rightleftarrows} \mathbf{L^b}Cu$	4.2(1)	468	6,800
$2\mathbf{L^b} + 2Cu \overset{\beta_{\mathbf{L^b}_2Cu_2}}{\rightleftarrows} \mathbf{L^b_2}Cu_2$	12.9(3)	468	14,000
$2\mathbf{L^b} + 3Cu \overset{\beta_{\mathbf{L^b}_2Cu_3}}{\rightleftarrows} \mathbf{L^b_2}Cu_3$	18.7(3)	468	17,000

[a] Solvent: $CH_3CN/H_2O/CH_2Cl_2$ (80/15/5, v/v/v); $T = 25.0(2)\,^\circ C$; $I = 0.1$ M. The errors are estimated to 1 nm for the wavelengths and to 5% for the extinction coefficients. For the sake of simplicity charges have been omitted in all the chemical equilibria.

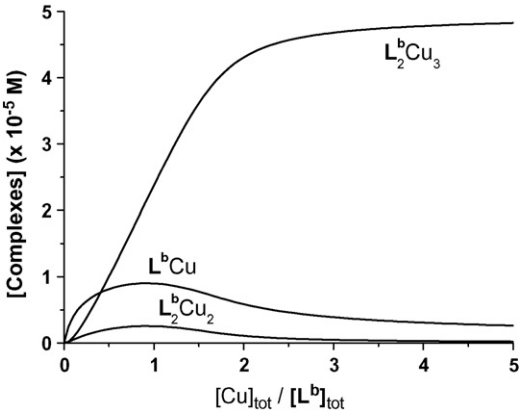

Fig. 4. Distribution curve related to the formation of cuprous complexes with $\mathbf{L^b}$. $[\mathbf{L^b}]_{tot} = 10^{-4}$ M. Solvent: $CH_3CN/H_2O/CH_2Cl_2$ (80/15/5, v/v/v); $T = 25.0(2)\,^\circ C$; $I = 0.1$; the stability constants are given in Table 1.

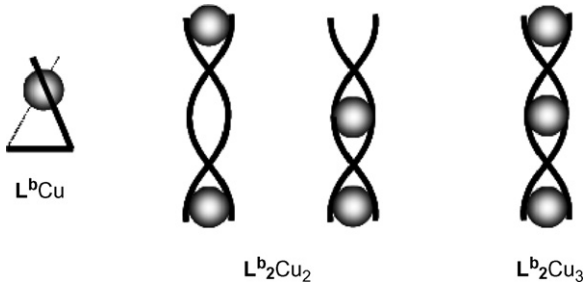

Fig. 5. Schematic representation of Cu^I complexes of $\mathbf{L^b}$.

a metal-to-ligand charge-transfer band (MLCT) in the visible region (λ_{max} = 460–470 nm) [23,45,46].

The stability of three cuprous $\mathbf{L^b}$ complexes were characterized at equilibrium, the mononuclear monostranded complex and the dinuclear and trinuclear bistranded species. For the sake of comparison, collected thermodynamic and spectrophotometric data for cuprous complexes formed with various bipyridine derivatives [47–49] are presented in Table 2.

Distribution curves in Fig. 4 clearly show the highly favored formation of the $\mathbf{L^b}_2Cu_3$ species, indicating appreciable positive cooperativity [50].

The copper(I) complexes of bipy and its derivatives give a broad intense MLCT band ($d\pi \rightarrow \pi^*$) in the visible (430–530 nm) [23,45,46]. The λ_{max} and the absorptivity of this band strongly depend on the substituents attached to the bipy moiety [51], which affect the geometry of the Cu^I complexes, the Cu–N bond length, and the electronic properties of the N-atoms [47,51,52]. An electron-withdrawing substituent shifts the absorption band to a lower frequency, whereas an electron-donating substituent raises the frequency [53]. The steric bulk of the substituents may cause lengthening of the Cu–N bond, leading to the destabilization of metal complexes, resulting in a poor back-bonding, and a compensatory blue-shift of the MLCT maximum [53]. Taking into account the electronic effects of the 4,4′-substituents ($CONEt_2$) as well as the effects of the steric bulk of these substituents, one may conclude that the differences in the spectrophotometric properties of the Cu^I complexes of $\mathbf{L'}$ and $\mathbf{L^b}$ (Table 2) are predominantly determined by steric effects.

Table 2
Global stability constants of Cu^I complexes with various bipyridine ligands

Ligand	$\log \beta$	λ_{max} (nm)	ε_{max} ($M^{-1}\,cm^{-1}$)
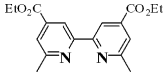 [a] [47]	$\log \beta_{\mathbf{LCu}} = 4.5$	380	3,380
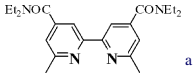 [a] [48]	$\log \beta_{\mathbf{L_2Cu}} = 8.6$	500 470	10,750 7,100
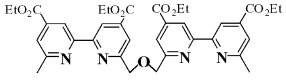 [a] [47]	$\log \beta_{\mathbf{L_2Cu_2}} = 14$	500	15,400
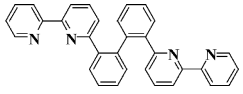 [b] [49]	$\log \beta_{\mathbf{LCu}} = 6.9$	465	4,400
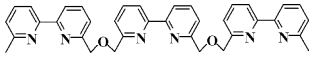 [a] [47]	$\log \beta_{\mathbf{L_2Cu_3}} = 20$	450	15,260

[a] CH_3CN/CH_2Cl_2 (50/50, v/v).
[b] CH_3CN.

The absorption spectra obtained for $\mathbf{L^b}Cu$, $\mathbf{L^b}_2Cu_2$ and $\mathbf{L^b}_2Cu_3$ clearly indicate the coordination of two bipy units to the copper centers. The only structure which can be proposed for $\mathbf{L^b}Cu$ is therefore the coordination provided by a folded ligand $\mathbf{L^b}$. The CH_2OCH_2 bridge is short enough to hinder tetrahedral binding of an ion by two consecutive bipy groups of the same ligand. We conclude that the Cu^I cation in $\mathbf{L^b}Cu$ is coordinated by the two external bipy. Such a folded structure has already been observed for the Cu^I species formed with 2,2′-bis(6-(2,2′-bipyridyl)biphenyl) [48]. The two $\mathbf{L^b}_2Cu_2$ and $\mathbf{L^b}_2Cu_3$ species are expected to be of double helicate type by analogy with the tricuprous species of its unsubstituted parent $\mathbf{L}'$, for which the double helicate structure was confirmed by X-ray crystallography [32]. The structures of these three Cu^I complexes with $\mathbf{L^b}$ are presented in Fig. 5.

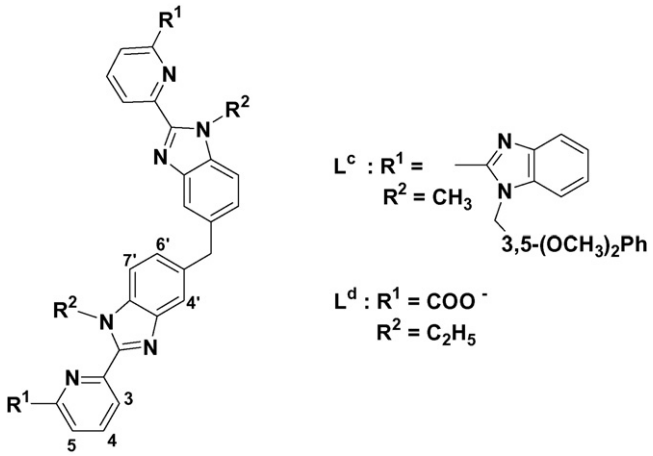

Fig. 6. Chemical structures of $\mathbf{L^c}$ and $\mathbf{L^d}$ strands.

2.3. Triple-stranded di-europium helicates

As we have seen in the previous examples, most of the studies devoted to double- or triple-stranded helicates based on cations involve Cu^I, Ag^I, Cu^{II}, Ni^{II} or Fe^{III} and strands bearing bipyridine, terpyridine, hydroxamate or catecholate binding sites [7,5,54]. The luminescent properties [55–57] of the lanthanide cations [58] are already taken advantage of in medical applications [59–61]. However, polymetallic lanthanide supramolecular complexes [62] may contribute to the development of more sensitive biosensors. In this context, the poor stereochemical preferences and the variable coordination numbers adopted by Ln(III) ions render difficult a reliable molecular programming in solution. In spite of this difficulty, we have demonstrated that a careful ligand design based on the induced fit principle [63] leads to the strict self-assembly of lanthanide-containing triple-stranded helicates in organic media [64–67]. The ditopic hexadentate ligand $\mathbf{L^c}$ derived from 2-pyridin-2-yl-1*H*-benzimidazole can be used to prepare bimetallic 3d–4f and 4f–4f assemblies (Fig. 6) [8,68]. Bioanalytical and medical applications require water-soluble probes, so that the ditopic strand $\mathbf{L^d}$ (Fig. 6) with two terminal carboxylate groups was synthesized [69,70].

In Fig. 7, the X-ray structures of the triple-stranded dinuclear Eu(III) helicates with $\mathbf{L^c}$ [64,71] and $\mathbf{L^d}$ [69] are presented.

In the case of $\mathbf{L^c}$, each strand involves two tridentate (*N*,*N*,*N*) moieties to bind europium(III). A combination of electrospray mass spectrometry and absorption spectrophotometry allowed the characterization of three complexes $\mathbf{L^c}Eu$, $\mathbf{L^c}_2Eu_2$ and $\mathbf{L^c}_3Eu_2$ in acetonitrile [68]. Examining the water-soluble analogue $\mathbf{L^d}$, a single Eu(III) species could be observed in water, by either absorption and emission spectrophotometries or ^1H NMR, the triple-stranded di-europium(III) helicate [70]. The corresponding stability constant is given in Table 3.

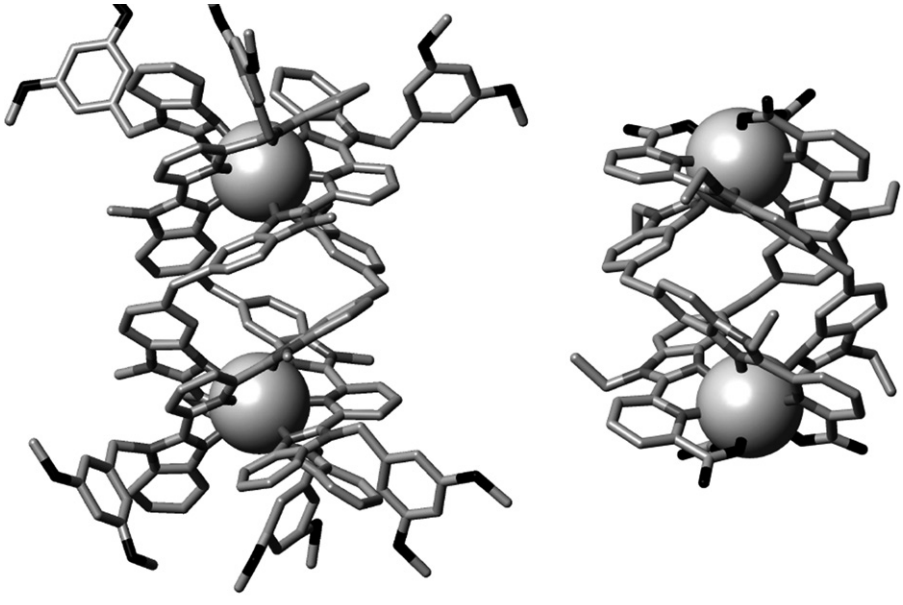

Fig. 7. X-ray structures of the triple-stranded dinuclear Eu(III) helicates with (a) $\mathbf{L^c}$ and (b) $\mathbf{L^d}$.

Table 3
Global stability constants of europium(III) complexes with $\mathbf{L^c}$ in CH_3CN and $\mathbf{L^d}$ in water[a]

Equilibrium	log β
$2\mathbf{L^c} + 2Eu \overset{\beta_{\mathbf{L^c}_2Eu_2}}{\rightleftarrows} \mathbf{L^c}_2Eu_2$	$\log \beta_{\mathbf{L^c}_2Eu_2} = 18.1(3)$
$3\mathbf{L^c} + 2Eu \overset{\beta_{\mathbf{L^c}_3Eu_2}}{\rightleftarrows} \mathbf{L^c}_3Eu_2$	$\log \beta_{\mathbf{L^c}_3Eu_2} = 24.3(4)$
$2\mathbf{L^c} + Eu \overset{\beta_{\mathbf{L^c}_2Eu}}{\rightleftarrows} \mathbf{L^c}_2Eu$	$\log \beta_{\mathbf{L^c}_2Eu} = 11.6(3)$
$3\mathbf{L^d} + 2Eu \overset{\beta_{\mathbf{L^d}_3Eu_2}}{\rightleftarrows} \mathbf{L^d}_3Eu_2$	$\log \beta_{\mathbf{L^d}_3Eu_2} = 51(2)$

[a] For the sake of simplicity charges have been omitted in all the chemical equilibria. $T = 25.0(1)\,^\circ C$; estimated errors = 3σ.

For the sake of comparison, we have collected in Table 4 stability constants determined for benzimidazole derivatives with Eu(III).

The most surprising result is the low stability of $\mathbf{L^c}Eu$, $K_{\mathbf{L^c}Eu}$ being 3–4 orders of magnitude lower than $K_{\mathbf{L^1}Eu}$ and $K_{\mathbf{L^2}Eu}$ in the same solvent. By contrast, the successive stability constant of $\mathbf{L^c}_2Eu$ is significantly higher than the corresponding parameters determined for the monotopic analogs $\mathbf{L}^1$ and $\mathbf{L}^2$ under identical experimental conditions [72,73]. The global stability constant of the bimetallic double-stranded complex $\mathbf{L^c}_3Eu_2$ is equal to 18.1(3), which is in agreement with the values determined elsewhere for similar systems [66,74]. The stability constant of $\mathbf{L^c}_2Eu_2$ ($\log \beta_{\mathbf{L^c}_3Eu_2} = 24.3(4)$) is about 2–4 orders of magnitude higher than the value estimated to $20 < \log \beta_{\mathbf{L^c}_3Eu_2} < 22$ in a previously published work [64], but it is close to the values determined for analogous helicates [66,67]. This difference can be traced back to the oversimplified model used to fit the data and to partial thermodynamic equilibrium of the sample's solutions in the preliminary study. Distribution diagram showed that the bimetallic helicate $\mathbf{L^c}_3Eu_2$ was the major complex under our experimental conditions in a large range of stoichiometries. This result indicates that, when europium(III) is not in excess with respect to $\mathbf{L^c}$, the self-assembly of $\mathbf{L^c}_3Eu_2$ exhibits positive cooperativity [75] as already mentioned for trimetallic double-stranded helicates with Cu^I [37,50] and Ag^I [76] and triple-stranded diferric complexes [54].

Table 4
Stepwise stability constants of europium(III) complexes formed with $\mathbf{L^c}$ and benzimidazole derivatives[a]

Equilibrium	log β
$\mathbf{L^c} + Eu \overset{K_{\mathbf{L^c}Eu}}{\rightleftarrows} \mathbf{L^c}Eu$	$\log K_{\mathbf{L^c}Eu} = 4.6(3)$[b]
$\mathbf{L^c}Eu + \mathbf{L^c} \overset{K_{\mathbf{L^c}_2Eu}}{\rightleftarrows} \mathbf{L^c}_2Eu$	$\log K_{\mathbf{L^c}_2Eu} = 7.0(4)$
$\mathbf{L^c}_2Eu + Eu \overset{K_{\mathbf{L^c}_2Eu_2}}{\rightleftarrows} \mathbf{L^c}_2Eu_2$	$\log K_{\mathbf{L^c}_2Eu_2} = 6.5(4)$
$\mathbf{L^c}_2Eu_2 + \mathbf{L^c} \overset{K_{\mathbf{L^c}_3Eu_2}}{\rightleftarrows} \mathbf{L^c}_3Eu_2$	$\log K_{\mathbf{L^c}_3Eu_2} = 6.2(5)$
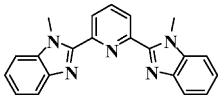 $\mathbf{L}^1$ [c]	$\log K_{\mathbf{L^1}Eu} = 9.0(2)$ $\log K_{\mathbf{L^1}_2Eu} = 6.7(3)$ $\log K_{\mathbf{L^1}_3Eu} = 6.9(4)$
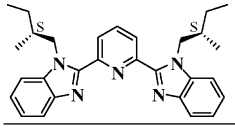 $\mathbf{L}^2$ [d]	$\log K_{\mathbf{L^2}Eu} = 8.2(2)$ $\log K_{\mathbf{L^2}_2Eu} = 5.9(3)$ $\log K_{\mathbf{L^2}_3Eu} = 4.0(5)$

For the sake of simplicity charges have been omitted; estimated errors = 3σ.
[a] Solvent: CH_3CN; $T = 25.0(1)\,^\circ C$.
[b] From kinetic data [68].
[c] From Ref. [72].
[d] From Ref. [73].

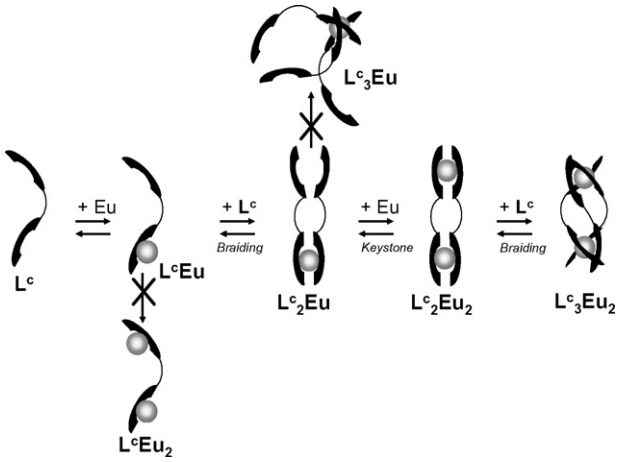

Fig. 8. Schematic representation of the proposed mechanism with strand $\mathbf{L^c}$.

In order to unravel the self-assembly mechanism of $\mathbf{L^c}_3Eu_2$, we have carried out kinetic measurements. We observed alternative "keystone" (addition of Eu(III)) and "braiding" (addition of strands) leading to the targeted edifice (Fig. 8). We did not observe any complex either with two Eu(III) bound to the same strand, because of too strong electrostatic repulsions, or with three strands bound to a single Eu(III) cation, because of the lack of reactivity of this intermediate on the way to helicates. Interestingly, the $\mathbf{L^c}_3Eu_2$ formation is mainly governed by electrostatic interactions. The kinetic studies clearly demonstrate that the apparent "magic", quantitative and fast self-assembly of five partners ($3\mathbf{L^c}$/2 Eu) into the final helicate $\mathbf{L^c}_3Eu_2$ is only observed under strict stoichiometric conditions with high reagent concentrations. Kinetic parameters [68] allowed us indeed to simulate the formation versus time of the Eu(III) species under various experimental conditions. These data pointed out the thermodynamic and kinetic behaviour of $\mathbf{L^c}_3Eu_2$, which is slowly and not significantly formed in excess of cation, but exclusively and rapidly obtained under stoichiometric conditions.

For the water-soluble ditopic $\mathbf{L^d}$ strand, which possesses tridentate (*N*,*N*,*O*) moieties, by contrast with $\mathbf{L^c}$, we could observe an intermediate $\mathbf{L^d}Eu_2$, since the two negative charges of the terminal carboxylate functions drastically reduce the electrostatic repulsions between the two Eu(III) cations (Fig. 9).

The kinetic results clearly demonstrated the key role of the bimetallic double-stranded species $\mathbf{L^d}_2Eu_2$. This species is very inert towards the release of either a ligand or a cation, but reacts very rapidly with an additional ligand strand to yield the final triple-stranded helicate. Indeed the formation of a 2:2 helical structure will decrease the steric hindrance and, moreover, the presence of negatively charged terminal carboxylate groups

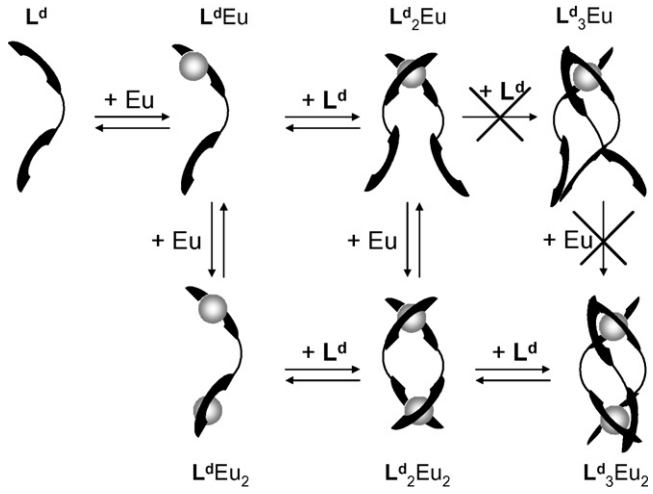

Fig. 9. Schematic representation of the self-assembly mechanism of $\mathbf{L^d}_2Eu$.

obviously contributes to prevent the formation a labile "side-by-side" [68,77] species. This is in contrast to the formation mechanism of $\mathbf{L^c}_3Eu_2$ for which we propose the formation of a labile intermediate $\mathbf{L^c}_2Eu_2$ [68]. The hexadentate ditopic ligand $\mathbf{L^d}$ leads to one of the most efficient cation/ligand system for the self-assembly of a bimetallic triple-stranded helicate in water. This is mainly due to the simultaneous presence of a short spacer and of one negative charge borne by each extremity.

3. Molecular switching devices

A specific case of controlled motion in molecular switches concerns the translocation of a metal ion between two different binding units within a same molecule. The directionally controlled motion of the cation is driven by an external stimulus according two possible scenarios: (i) the metallic cation exists in two oxidation states, each of them being firmly bound by its affine binding unit. Chemical or electrochemical oxidation–reduction processes thus triggers its reversible motion between the two distinct but complementary compartments; (ii) the properties of one binding site are modified through addition of H^+ or OH^-, and thereby induce an intramolecular metal translocation depending on its state of protonation and affinity for a given metallic ion. We will give here two examples of redox- and proton-driven molecular switches [78,79].

3.1. Redox-driven Cu^I/Cu^{II} molecular switch

In collaboration with Shanzer's group, we have reported a conformational redox molecular switch based on a double-stranded ditopic ligand $\mathbf{L^e}$ [78], which operates through the Cu^I/Cu^{II} pair (Fig. 10). This device is characterized by the presence of two binding compartments, a medium bis(8-hydroxyquinoline) coordinating moiety (N_2O_2) which preferentially coordinates Cu^{II} and a soft bis(2,2′-bipyridyl) binding site (N_4) that selectively prefers Cu^I ions (Fig. 10).

The thermodynamics [80–82] of 8-hydroxyquinoline (oxine; noted **8HQ**) and 2,2′-bipyridine (noted **Bpy**) model ligands with Cu^{II} and Cu^I, respectively, predict that the *N*,*O*-binding site in

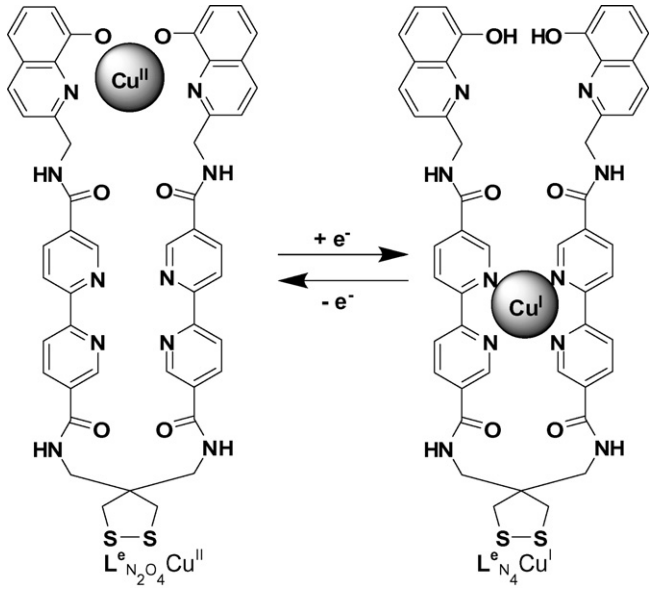

Fig. 10. Chemical structures and notation of cupric ($\mathbf{L^e}_{N_2O_4}Cu^{II}$) and cuprous ($\mathbf{L^e}_{N_4}Cu^I$) complexes of ligand $\mathbf{L^e}$.

$\mathbf{L^e}$ is a stronger ligand for cupric ion with respect to bipyridine, while an interesting contrast stands for cuprous cation (Table 5).

The electronic spectra of the cupric and cuprous complexes support these hypotheses. The absorption spectrum of $\mathbf{L^e}_{N_2O_2}Cu^{II}$ (Fig. 11) displays an intense shoulder at 398 nm ($\varepsilon_{398} = 3700(400)\ M^{-1}\ cm^{-1}$) on the absorption band of the ligand centered at 302 nm. Similarly, it is observed in $CHCl_3$ that the Cu^{II} binding induces a red shift to 412 nm of the absorption band of 8-hydroxyquinoline (310 nm) [83]. The electronic spectrum of $\mathbf{L^e}_{N_4}Cu^I$ (Fig. 11) shows an absorption band with a less intense shoulder at 480 nm ($\varepsilon_{480} = 2400(200)\ M^{-1}\ cm^{-1}$), which corresponds to the MLCT band of bis(2,2′-bipyridyl)Cu^I systems [21].

The reversible motion of the metal ion between the two compartments was driven by auxiliary oxidation (*tert*-butyl hydroperoxide) and reduction (ascorbic acid) reactions. The oxidation and the reduction reactions were found to be faster than the translocation process of Cu^I or Cu^{II}, and allowed us to separately follow the intramolecular movement of the copper cation. Using a stopped-flow technique and a spectrophotometric detection, we were able to confirm the reduction mechanism of cupric

Table 5
pCu values calculated for bipyridine and 8-hydroxyquinoline model ligands[a]

Ligands	pCu^{II}	pCu^I
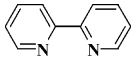	10.0[b]	**10.0**[c]
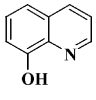	**12.8**[b]	6.2[b]

[a] $pCu = -\log[Cu]_{free}$; $[Cu]_{tot} = 10^{-6}$ M; $[Ligand]_{tot} = 10^{-5}$ M.
[b] $I = 0.1$ M, water.
[c] Solvent dioxane/water (50/50, v/v).

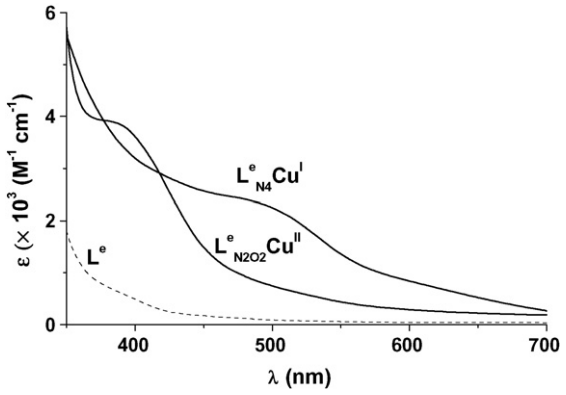

Fig. 11. Electronic spectra of ligand $\mathbf{L^e}$ and of its cupric and cuprous complexes. Solvent: 20 mM MES in DMF/water (80/20, v/v), pH* 6.0, $T = 25.0(2)\,^{\circ}C$, $l = 1$ cm.

complex by ascorbic acid [84] as well as the oxidation process of cuprous species by *tert*-butyl hydroperoxide [85]. The first-order rate constants relative to the slower step, which was easily attributed to the induced intramolecular motion of the copper cation, were determined. The chemically triggered redox switch reversibly interconverts with respective first-order rate constants of $k_I = 2.3(2) \times 10^{-2}\ s^{-1}$ for $*\mathbf{L^e}_{N_2O_2}Cu^I \rightarrow \mathbf{L^e}_{N_4}Cu^I$ and $k_{II} = 9(2) \times 10^{-4}\ s^{-1}$ for $*\mathbf{L^e}_{N_4}Cu^{II} \rightarrow \mathbf{L^e}_{N_2O_2}Cu^{II}$ under our experimental conditions (Scheme 1).

Although a large number of redox molecular machines was described up today, there are very few detailed kinetic studies on the mechanism of molecular motions available. Table 6 summarizes first-order rate constants for metal ion motion for various redox molecular switches [15,78,87–93]. It is noteworthy that the turnover of ion translocation varies from hundreds of milliseconds to several hours depending on the nature of ligand and metal. Since our ultimate objective was to design a molecular switch that would discriminate between its two states, and in which the change of the state would be fast and easily controlled [86], we will discuss the parameters which can be tuned to yield the targeted properties.

The selectivity of a switch, *i.e.* the preferential binding of the oxidized form of a metal ion in one coordination site and the reduced form of the ion in the complementary site, can be modulated by changes in stability of the respective complexes. For instance, in the case of $\mathbf{L^e}$, it would be desirable to bind Cu^{II} ion in the bis(8-hydroxyquinoline) coordination compartment only. The comparison of stability constants for bis(oxinate)Cu^{II} and

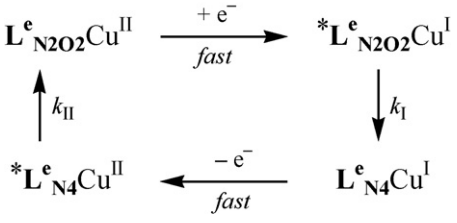

Scheme 1. Functioning principle of the redox-driven molecular switch. $*\mathbf{L^e}_{N_2O_2}Cu^I$ and $*\mathbf{L^e}_{N_4}Cu^{II}$: intermediates formed after reduction (oxidation) reaction; $\mathbf{L^e}_{N_2O_2}Cu^{II}$ and $\mathbf{L^e}_{N_4}Cu^I$: thermodynamic complexes. Solvent: 20 mM MES in DMF/water (80/20, v/v), pH* 6.0, $T = 25.0(2)\,^{\circ}C$.

Table 6
Turnover numbers ($1/k$) of metal ion translocation within various redox molecular switches

Switches	Pair	T_{red} [a]	T_{ox} [a]
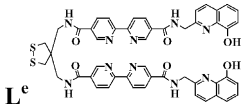 [b] [78]	Cu^{II}/Cu^I	44 s	18.3 min
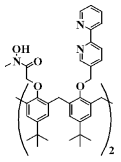 [c] [87]	Fe^{III}/Fe^{II}	41.7 min	–
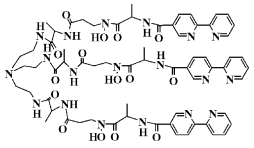 [d] [88,89]	Fe^{III}/Fe^{II}	18.3 min	–
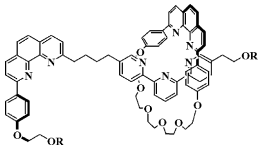 [e] [90]	Cu^{II}/Cu^I	100 s to 167 min	110 min
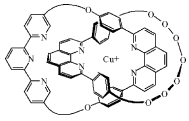 [e] [91]	Cu^{II}/Cu^I	∼1 s	13.9 h
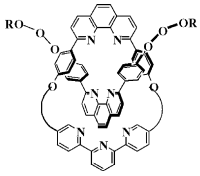 [f] [92]	Cu^{II}/Cu^I	650 ms	1.40 s
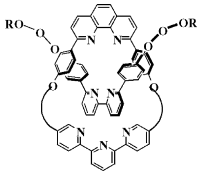 [e] [15]	Cu^{II}/Cu^I	2 ms	200 ms
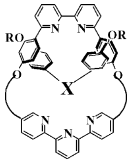 [g] [93]	Cu^{II}/Cu^I	Fast	(**1**) 10 s (**2**) 1 s (**3**) 200 ms

[a] The turnover numbers T_{red} and T_{ox} correspond to the translocation after reduction and oxidation, respectively at 25 °C.
[b] DMF/0.1 M MES (80/20, v/v), pH* 6.0.
[c] CH_3OH/0.1 M MES (80/20, v/v), pH 6.2.
[d] CH_3OH/0.5 M tris (50/50, w/w), pH 8.0.
[e] CH_3CN, $I = 0.1$ M (n-Bu_4NBF_4).
[f] CH_3CN/CH_2Cl_2 (80/20, v/v), $I = 0.1$ M (n-Bu_4NBF_4).
[g] CH_3CN/CH_2Cl_2 (90/10, v/v), $I = 0.1$ M (n-Bu_4NBF_4). (**1**) X = Phen; (**2**) X = Bipy; (**3**) X = 3,3′-biisoquinoline.

bis(2,2′-bipyridyl)Cu^{II} illustrates that cupric ion will be preferentially bound to the bis(oxinate) component of the switch (Table 5). Moreover, the electron-withdrawing amide groups attached to the 2,2′-bipyridyl moiety decrease electron density on the pyridine *N*-atoms and make them less willing to bind hard cupric ion [94]. Similarly, Cu^{I} is preferentially bound in the bis(2,2′-bipyridyl) cavity. It is noteworthy that higher is the specificity of a coordination site for one oxidation state of the metal ion compared to the other oxidation state, stronger reduction (or oxidation) reagent must be used for triggering the switch. Reduction of $\mathbf{L^e}_{N_2O_2}Cu^{II}$ complex can be given as an example. The reaction is written:

$$\mathbf{L^e}_{N_2O_2}Cu^{II} \xrightarrow{+e^-} \mathbf{L^e}_{N_2O_2}Cu^{I} \quad (6)$$

The standard reduction potential E^0 for reaction (6) is given:

$$E^0 = \frac{RT}{F} \ln \frac{[\mathbf{L^e}_{N_2O_2}Cu^{I}]}{[\mathbf{L^e}_{N_2O_2}Cu^{II}]} \quad (7)$$

The equilibrium concentrations $[\mathbf{L^e}_{N_2O_2}Cu^{I}]$ and $[\mathbf{L^e}_{N_2O_2}Cu^{II}]$ are given by the following equations:

$$[\mathbf{L^e}_{N_2O_2}Cu^{I}] = \beta_I[Cu^{I}][\mathbf{L^e}] \quad (8)$$

$$[\mathbf{L^e}_{N_2O_2}Cu^{II}] = \beta_{II}[Cu^{II}][\mathbf{L^e}] \quad (9)$$

where β_I and β_{II} are stability constants for $\mathbf{L^e}_{N_2O_2}Cu^{I}$ and $\mathbf{L^e}_{N_2O_2}Cu^{II}$ complexes, respectively. Substituting Eqs. (8) and (9) into Eq. (7) thus led to

$$E^0 = \frac{RT}{F} \ln \frac{\beta_I[Cu^{I}]}{\beta_{II}[Cu^{II}]} \quad (10)$$

Using the standard reduction potential of the Cu^{II}/Cu^{I} couple led to

$$E^0_{Cu^{II}/Cu^{I}} = \frac{RT}{F} \ln \frac{[Cu^{I}]}{[Cu^{II}]} \quad (11)$$

Therefore Eq. (5) can be written as

$$E^0 = \frac{RT}{F} \ln \frac{\beta_I}{\beta_{II}} + E^0_{Cu^{II}/Cu^{I}} \quad (12)$$

Now it becomes obvious that for lower β_I/β_{II} ratio, the coordination site will be more selective with respect to the Cu^{II} ion, but the reduction potential of the $\mathbf{L^e}_{N_2O_2}Cu^{II}$ complex will decrease, thus imposing the use of a stronger reduction agent. This does not have to cause a problem when triggering the switch electrochemically, but can be a limiting factor for a chemically triggered switch.

Besides, another important aspect of such molecular switches is the rate of the cation translocation or, generally speaking, the rate of the coordination sphere exchange. The overall process can be divided into several stages: (i) breaking of some coordination bonds between the ligand and the metal ion, (ii) change in the complex geometry, which can consist of conformational changes (anchored bipodal or tripodal switches) or motion (translation, rotation, rocking) of non-covalently bound parts of the system (catenates and rotaxanes) and (iii) formation of new metal–ligand bonds. This sequence can be iterated several times if stable kinetic intermediates are produced [95].

Thermodynamics is the driving force of the rate of the first and third step. Indeed, after the oxidation state variation of the metal ion, the metal–ligand bond dissociation is expected to be fast if the stability of the resulting complex is lower due to geometric constrains or inadequate electronic requirements. Similarly, high formation rate of the new metallic species will accelerate the ion translocation. Nevertheless, an important factor is the ability of an ion to undergo fast ligand exchanges, which can be anticipated from solvent exchange rates. For example, water exchange rate for $[Cu^{II}(H_2O)]^{2+}$ ion is $k_{ex} \approx 10^{10}\ s^{-1}$, while that of $[Fe^{III}(H_2O)]^{3+}$ is $1.6 \times 10^2\ s^{-1}$ [96]. These kinetic data strongly suggest that copper-based switches should proceed faster in ion translocation than those based on iron as illustrated in Table 6.

The rate of the second stage of the metal translocation process will depend on the activation barrier imposed to the process. For instance, in the case of $\mathbf{L^e}$, the oxinate moiety is substituted through a sp^3 carbon atom to the amide linkage. This allows free rotation of the binding unit and easier approach to the 2,2′-bipyridyl group of the adjacent arm. Another relevant example is the triple-stranded Fe^{III}/Fe^{II} switch based on hydroxamate and 2,2′-bipyridyl cavities (Table 6) [88]. The rate constant for iron(II) translocation is $k_{red} = 9(1) \times 10^{-4}\ s^{-1}$ (Table 6), while for its homologues possessing shorter spacers between the hydroxamate and 2,2′-bipyridyl moieties (instead of $–CH_2–CH_2–$ spacer, a $–C^*H(CH_3)–$ group was used), the rate constant k_{red} was found to be equal to $1.9(2) \times 10^{-3}\ s^{-1}$ and $2.2(2) \times 10^{-3}\ s^{-1}$ for *R*- and *S*- absolute configurations, respectively [88,89]. The shortening of the spacers consequently led to higher rates of translocation. Besides, in the case of the pseudo-rotaxanes (Table 6), it was shown that the flexibility of the threaded chelate and the low steric hindrance of its coordination moiety allowed to significantly increase the speed of the pirouetting motion [93].

Another important issue in ion translocation within molecular switches is a possible role of *a priori* non-coordinating groups, such as amide linkages. It can be suggested that these amide spacers assist the ion translocation and thus decrease the energy barrier for the overall process. Detailed kinetic studies of analogous ligands of $\mathbf{L^e}$ with structural variations on the spacers would contribute to a better understanding of these mechanisms.

Lastly, the solvent and/or other ions (counter ions, background salt) could also play a non-innocent role on the rate of the ion translocation in a given switch [91], and can be thus used for fine tuning the performance of the system.

If numerous molecular switches have been described in the literature, very little is known about the functioning and dynamics of such systems. Our kinetic approach allowed to unravel the metal translocation mechanism within a bipodal ligand $\mathbf{L^e}$ and pointed out that several structural, energetic, steric and kinetic criteria which should be taken into account to design new systems with improved efficiencies and speeds.

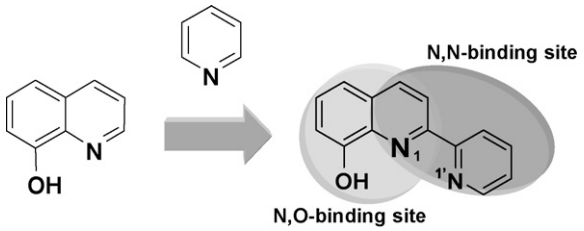

Fig. 12. Chemical structure of ligand $\mathbf{L^f}$.

3.2. Proton-driven multistate Ni^{II} molecular switch

The successful work undertook on $\mathbf{L^e}$ encourages us to design closely related and more efficient systems by introducing the two binding functionalities (oxinate and 2,2′-bipyridine) into a single molecule $\mathbf{L^f}$ (Fig. 12). Pyridine was chosen as the simplest and most basic substituents which could be introduced in position 2 of a 8-hydroxyquinoline backbone. This directionally oriented synthesis confers to $\mathbf{L^f}$ potential binding properties of either bidentate or tridentate unit.

Due to the presence of multi-compartmental binding sites sharing a common coordinating moiety (central pyridine), and to the conformational properties of the 2,2′-bipyridyl unit (*cis* and *trans* conformers), $\mathbf{L^f}$ is anticipated to operate like a redox or proton-driven multistage molecular switching device based on region-selective metal binding [97]. This molecular design indeed offers a potential control of the ionic recognition process, which could be easily triggered by external stimuli. Interestingly, thermodynamics of oxinate and 2,2′-bipyridine model ligands with a divalent cation demonstrate that the *N*,*O*-binding site (oxinate) is preferred at high pH, while that of the *N*,*N*-bipyridine leads to more stable complexes under acidic conditions. This system has the advantage to combine the coordination properties of these two individual but complementary units in order to form stable complexes in large span of pH.

A spectrophotometric and potentiometric titration conducted on free $\mathbf{L^f}$ allowed us to determine two of its three protonation constants ($\log K_1^H = 10.9(1)$ and $\log K_2^H = 3.18(5)$). The electronic spectra of the protonated species of $\mathbf{L^f}$ are given in Fig. 13.

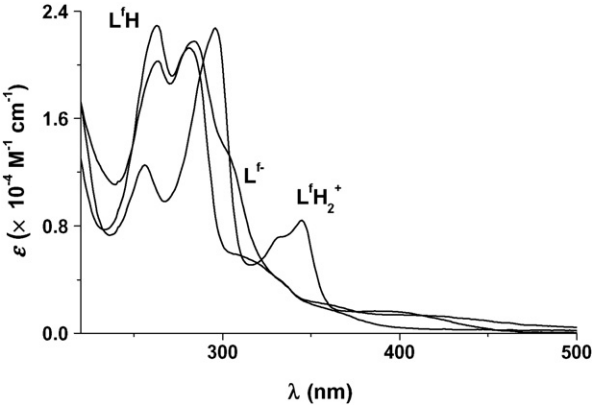

Fig. 13. Electronic spectra of protonated species of the ligand $\mathbf{L^f}$. Solvent: CH_3OH/H_2O (80/20 wt%); $I = 0.1$ M (NEt_4ClO_4); $T = 25.0(2)$ °C.

The first protonation was easily attributed to the phenolate function, and is characterized by the loss of the broad shoulder centered at 303 nm, together with a hyperchromic increase of the absorption band lying at higher energies ($\lambda_{max} = 263$ nm; $\varepsilon_{263} = 2.29 \times 10^4\ M^{-1}\ cm^{-1}$). The second protonation of the N1′-pyridine of $\mathbf{L^f}$ induces significant spectrophotometric variations with the formation of intense splitted absorption bands at 333 ($\varepsilon_{333} = 7.20 \times 10^3\ M^{-1}\ cm^{-1}$) and 345 nm ($\varepsilon_{345} = 8.43 \times 10^3\ M^{-1}\ cm^{-1}$) and a concomitant bathochromic shift of 15 nm ($\lambda_{max} = 296$ nm; $\varepsilon_{296} = 2.27 \times 10^4\ M^{-1}\ cm^{-1}$) of the absorption band centered at 281 nm. These spectrophotometric data strongly suggest a *trans*-to-*cis* conformational change of the *N*,*N*-bipyridyl moiety, which could be stabilized by intramolecular hydrogen bonds involving the three heteroatoms of $\mathbf{L^f}$. These absorption bands were attributed to short-axis (π_2) and long-axis (π_1) polarized π–π^* transitions. The splitting and bathochromic shifts of the long-axis polarized transitions (π_1) was rationalized by rotational interconversion between the two conformers (*cis*-$\mathbf{L^f}H_2^+$ and *trans*-$\mathbf{L^f}H$) which is triggered by protonation. Interestingly, $\mathbf{L^f}$ possesses informative spectroscopic probes to emphasize the nature of the protonation site, as well as the possible conformational arrangements adopted by the corresponding protonated species. The use of electrospray mass spectrometry to characterize the stoichiometry of metallic complexes in solution is well documented [5,35,36,68], and has been employed by us for this purpose on previous occasions [22,37,54,68,98]. In order to establish the stoichiometries of the nickel(II) complexes formed with $\mathbf{L^f}$, ESMS+ spectra were recorded with ligand concentrations equal to 2.0×10^{-5} M, and with final $[Ni]_{tot}/[\mathbf{L^f}]_{tot}$ ratios equal to 10 and 0.5 (Fig. 14).

The ESMS+ spectra of the various solutions were analyzed, and the conclusive assignments of the different peaks were done by comparing the experimental isotopic patterns with the corresponding simulated profiles. Two complexes, $\mathbf{L^f}Ni$ and $\mathbf{L^f}_2Ni$, could be clearly evidenced. In addition, two peaks with high-masses corresponding to $[3\mathbf{L^f} + 2Ni]^+$ and $[2\mathbf{L^f} + 2Ni + ClO_4]^+$ were also observed. The ionization of these metal complexes was mainly obtained by addition or loss of protons and by addi-

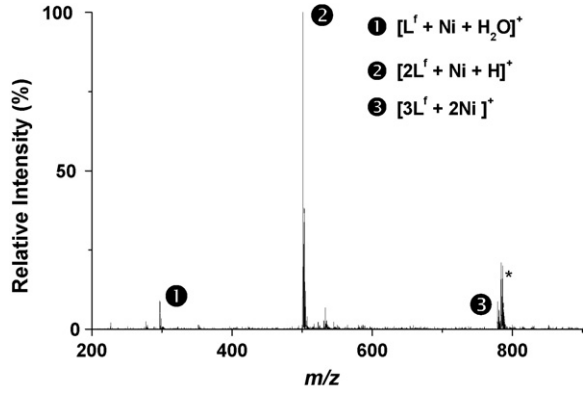

Fig. 14. ESMS+ spectra of nickel(II) complexes formed with $\mathbf{L^f}$. Solvent: methanol/water (80/20 wt%); positive mode ESMS+. $[\mathbf{L^f}]_{tot} = 2.0 \times 10^{-5}$ M; $[Ni(II)]_{tot} = 10^{-5}$ M; $V_{cap.exit} = 240$ V; $V_{trap\ drive} = 55$ V; *impurity $[3\mathbf{L^f} + Cu + Ni]^+$. For the sake of clarity, $\mathbf{L^f}$ stands for the fully deprotonated ligand.

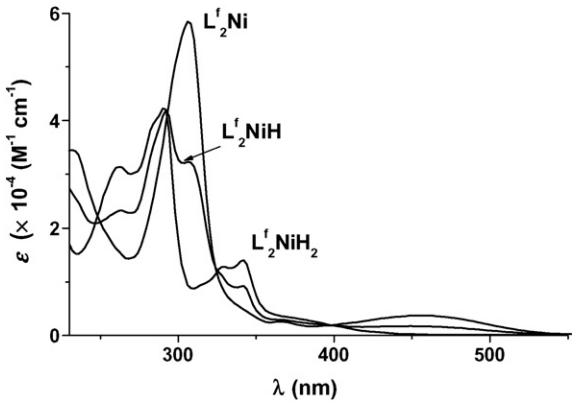

Fig. 15. Electronic spectra of the Ni(II) complexes formed with $\mathbf{L^f}$. Solvent: methanol/water (80/20 wt%); $I = 0.1$ M (NEt_4ClO_4); $T = 25.0(2)$ °C.

tion of perchlorate counter-anions. Probably due to weak ESMS responses, the monochelate $\mathbf{L^f}$Ni was often found as a minor species except in excess of the metal. For $\mathbf{L^f}$Ni, the presence of a bound water molecule supports the unsaturated character of the coordination shell.

The Ni(II) coordination properties of the molecular building block $\mathbf{L^f}$ were further investigated by spectrophotometric and potentiometric titrations. A model with a mononuclear species containing two ligands, $\mathbf{L^f}_2$Ni ($\log \beta \mathbf{L^f}_2\mathrm{Ni} = 25.3(3)$), satisfactorily adjusts the spectrophotometric data, in agreement with the ESMS study. In addition, two protonated species, $\mathbf{L^f}_2$NiH ($\log K_{\mathbf{L^f}_2\mathrm{NiH}} = 5.3(3)$) and $\mathbf{L^f}_2\mathrm{NiH}_2$ ($\log K_{\mathbf{L^f}_2\mathrm{NiH}_2} = 3.2(4)$) can be also evidenced. The electronic spectra of the Ni(II) species with $\mathbf{L^f}$ are given in Fig. 15.

Despite differences in solvent, these values agree with those determined elsewhere [99] in dioxane/water (50/50, v/v). It is noteworthy that, under our experimental conditions, the major difference is the absence of significant amounts of mononuclear monochelates in solution, which precludes any accurate determination of their respective affinities. $\mathbf{L^f}$Ni complex was nevertheless detected by mass spectrometry. To further confirm this observation, spectrophotometric titrations at p[H] 2.0 and in excess of metal were carried out and allowed to determine conditional stability constant ($\log K^*_{\mathbf{L^f}\mathrm{Ni}} = 4.3(2)$) of the monochelate. This value was compared to data available in the literature ($\log K^*_{\mathbf{L^f}\mathrm{Ni}} = 3.77$) [99]. The protonation constants of the bischelate complexes ($\log K_{\mathbf{L^f}_2\mathrm{NiH}}$ and $\log K_{\mathbf{L^f}_2\mathrm{NiH}_2}$) most likely correspond to the phenolate groups as shown by the spectrophotometric data (Fig. 15). These values are lower of ≈5 to ≈8 orders of magnitude with respect to free $\mathbf{L^f}$, mainly due to electronic effects resulting from the coordination processes. The distribution diagrams of the Ni(II) complexes with $\mathbf{L^f}$ are given in Fig. 16.

To emphasize the peculiar binding properties of $\mathbf{L^f}$, pNi values [100] were calculated at three selected p[H] values (3, 5 and 9). These pNi values were compared to those calculated for 2,2′-bipyridine [31,101] and 8-hydroxyquinoline [102] models. Interestingly, these thermodynamic data point out that $\mathbf{L^f}$ combines the advantages of a bipyridine coordination unit at acidic p[H] and of a 8-hydroxyquinoline binding site at higher p[H].

Table 7
pNi[a] values calculated at p[H] 3.0, 5.0 and 9.0 for the Ni(II) complexes with 2,2′-bipyridine (**Bpy**)[b], 8-hydroxyquinoline (**8HQ**)[b] and ligand $\mathbf{L^f}$ [c]

pNi	p[H] = 3.0		
	Bpy	**8HQ**	$\mathbf{L^f}$
pH 3	**7.0**	6.0	**7.33**
pH 5	**10.4**	6.1	**9.8**
pH 9	10.72	**12.9**	**17.3**

[a] $\mathrm{pNi} = -\log[\mathrm{Ni}]_{\mathrm{free}}$ with $[\mathrm{Ligand}]_{\mathrm{tot}} = 10^{-5}$ M and $[\mathrm{Ni}]_{\mathrm{tot}} = 10^{-6}$ M.
[b] Solvent: water; $I = 0.1$ M (KCl); $T = 25$ °C.
[c] Solvent: methanol/water (80/20 wt%); $I = 0.1$ M (NEt_4ClO_4); $T = 25.0(2)$ °C.

Under acidic conditions, the *cis*-bipyridyl unit is the preferred coordination site for Ni(II), as shown by the electronic spectra of $\mathbf{L^f}_2\mathrm{NiH}_2$ (Fig. 15). We previously demonstrated that $\mathbf{L^f}$ possesses valuable spectroscopic probes to highlight the protonation site which is involved, as well as the conformational arrangement adopted by the corresponding protonated species. The same spectroscopic signatures can be also exploited to emphasize the nature and the conformation of the metallic complexes. As an example, the fine vibronic structure of the absorption bands centered at 330 nm and 342 nm (333 nm and 345 nm for $\mathbf{L^f}\mathrm{H}_2$) and the sharp and intense transitions at 292 nm (296 nm for fo $\mathbf{L^f}\mathrm{H}_2$) of $\mathbf{L^f}_2\mathrm{NiH}_2$ are strong indications of the *cis*-arrangement adopted by each bipyridyl-type binding unit. The pNi values of the metallic complexes with $\mathbf{L^f}$ at p[H] 3 confirm these coordination properties as shown by the similar values with the **Bpy** model. The comparison with the pNi values of **8HQ** model demonstrates that the *N*,*O*-bidentate binding unit is unable to compete with the *N*,*N*-bidentate coordination site of $\mathbf{L^f}$ under such conditions (Fig. 12). The increase of the p[H] induces the successive deprotonation of the bischelate species and triggers a drastic change of the coordination properties with the two *N*,*O*-binding sites being now involved in the binding processes. Indeed, at basic p[H] = 9, the oxinate ligands become more powerful binding units than bipyridines. Consequently, the metal is displaced to its thermodynamically favored compartment (Table 7). Thereby, thermodynamics of **Bpy**-Ni(II) and **8HQ**-Ni(II) is the major driving force of the proton-driven switch $\mathbf{L^f}$. When the p[H] increases, the spectro-

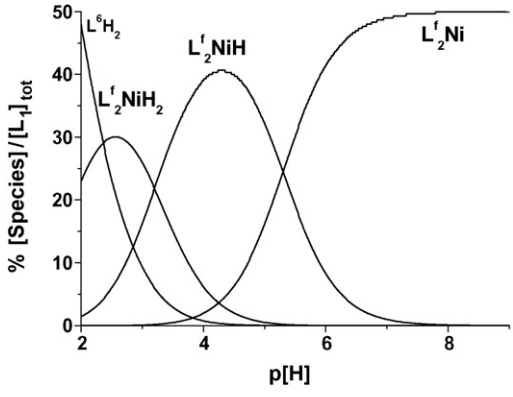

Fig. 16. Distribution diagrams of nickel(II) complexes with $\mathbf{L^f}$ as a function of p[H]. Solvent: methanol/water (80/20 wt%); $I = 0.1$ M (NEt_4ClO_4); $T = 25.0(2)$ °C; $[\mathbf{L^f}]_{\mathrm{tot}} = 3.0 \times 10^{-5}$ M, $[\mathrm{Ni}]_{\mathrm{tot}} = 1.5 \times 10^{-5}$ M.

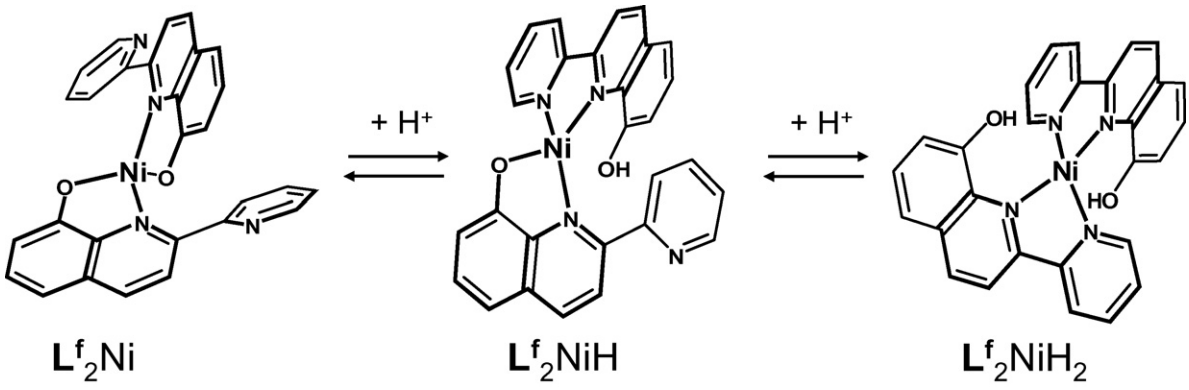

Fig. 17. Schematic representation of the three states structural switching of bischelate complexes based on ligand $\mathbf{L^f}$ which operate by successive protonations.

scopic mark of the *cis*-arrangement of the bipyridyl component gradually disappears with a simultaneous formation and increase of an intense absorption band at ≈306 nm, which is characteristic of the bis(oxinates)Ni(II) complex [103,104]. Moreover, $\mathbf{L^f}_2$NiH and $\mathbf{L^f}_2$Ni display a weak and broad absorption band in the visible region, which is related to tautomeric forms of the 8-hydroxyquinolinate pattern [103]. These spectrophotometric observations point out two *cis*-to-*trans* conformation changes of the terminal N1′-pyridine (Fig. 16).

Depending on the p[H] conditions, $\mathbf{L^f}$ possesses two individual and complementary bidentate binding boxes, namely the *N*,*N*-bipyridine and the *N*,*O*-oxinate. Ligand $\mathbf{L^f}$ operates either as *N*,*N*- or as *N*,*O*-bidentate binder, and these coordination processes are reversibly triggered by the proton. The existence of three stable and reversible states with distinguishable spectroscopic properties, *i.e.* the three protonated species of the bischelate, and their reversible interconversions by p[H] changes, confers to $\mathbf{L^f}$ molecular switch properties. It can be therefore considered as a "*three states molecular switch*" (Fig. 17) [15,78].

4. Conclusions

We have presented here original research results which allowed to unravel the self-assembling mechanism in solution of two to three polytopic strands bound to two to three cations. All of the four helicates presented here are driven by thermodynamics *via* labile or inert intermediates. The helical structures are diminishing the electrostatic repulsions between the cations. Positive intramolecular interactions are necessary to lead to the targeted edifice and to render the self-assembly process "magic" which means fast and quantitative. But, the whole mechanism could go on "narrow roads" at low concentrations or at inappropriate ratios in ligand and metal concentrations. In this case, slow self-assembly processes, which produce intermediate complexes, could be observed. Interestingly, our results showed that the hexadentate ditopic ligand $\mathbf{L^d}$ led to one of the most efficient cation/ligand system for the self-assembly of a helicate in water. This was essentially due to the simultaneous presence of a short spacer and of one negative charge borne by each extremity.

A molecular switch based on a double-stranded ditopic ligand $\mathbf{L^e}$, which operates through the Cu(I)/Cu(II) couple [78], was also described. The reversible motion of the copper ion between the two binding sites was triggered by auxiliary oxidation and reduction reactions. Our kinetic approach allowed to unravel the metal translocation mechanism and to evaluate the rates of the translocation motions. Combination of these two binding functionalities (bipyridine and oxinate) into a single molecule $\mathbf{L^f}$ induces new properties. Indeed, the binding and conformational properties of that system confer a potential of proton-driven multistate molecular switch. Our results broaden the knowledge on the self-assembly processes of supramolecular edifices, and pave the way to a better understanding of the signal propagation and conformational changes within new functional molecular devices.

Acknowledgements

This work has been supported by the Center National de la Recherche Scientifique (UMR 7177). The authors express their thankfulness to our co-workers for their outstanding contributions, their names being cited in the references. Fruitful and active collaborations with renowned and leading groups (Profs. J.C.G. Bünzli (Lausanne, Switzerland), J.M. Lehn (Strasbourg, France), C. Piguet (Geneva, Switzerland), J.L. Pierre (Grenoble, France) and A. Shanzer (Rehovot, Israel)) made this enthusiastic and multidisciplinary research possible. We would like to thank all of them for their enthusiasm, support, discussions and contributions.

References

[1] J.M. Lehn, Supramolecular Chemistry—Concepts and Perspectives, VCH, Weinheim, 1995 (and references cited therein).
[2] J.E. Vaener (Ed.), Self-Assembly Architecture, A.R. Liss, New York, 1988;
D. Philp, J.F. Stoddart, Angew. Chem. Int. Ed. Engl. 35 (1996) 1155;
P.N.W. Baxter, Comprehensive Supramolecular Chemistry, Pergamon Press, Oxford, 1996 (Chapter 6);
M. Fujita, Comprehensive Supramolecular Chemistry, Pergamon, Oxford, 1996 (Chapter 7);
F. Vögtle, Supramolecular Chemistry, John Wiley & Sons, Chichester, 1991;
G.M. Whitesides, J.P. Mathias, C.T. Seto, Science 254 (1991) 1312.
[3] P.W. Kuchel, G.B. Ralston, Biochemistry. Schaum's Outline Series, McGraw Hill, New York, 1988, p. 91;

S. Leininger, B. Olenyuk, P.J. Stang, Chem. Rev. 100 (2000) 853;
C.P. McArdle, M.J. Irwin, M.C. Jennings, R.J. Puddephat, Angew. Chem. Int. Ed. Engl. 38 (1999) 3376;
R.E. Gillard, F.M. Raymo, J.F. Stoddart, Chem. Eur. J. 3 (1977) 1933.
[4] G.F. Swiegers, T.J. Malefetse, J. Incl. Phenom. Macrocycl. Chem. 40 (2001) 253;
G.F. Swiegers, T.J. Malefetse, Chem. Rev. 100 (2000) 3483;
M. Fujita, Acc. Chem. Res. 32 (1999) 53.
[5] C. Piguet, G. Bernardinelli, G. Hopfgartner, Chem. Rev. 97 (1997) 2005.
[6] J.P. Sauvage, Chem. Commun. (2005) 1507;
J.P. Collin, J.P. Sauvage, Chem. Lett. 34 (2005) 742;
J.P. Collin, V. Heitz, S. Bonnet, J.P. Sauvage, Inorg. Chem. Commun. 8 (2005) 1063;
J.P. Collin, V. Heitz, J.P. Sauvage, Top. Curr. Chem. 262 (2005) 29.
[7] M. Albrecht, Chem. Rev. 101 (2001) 3457.
[8] J.C.G. Bünzli, C. Piguet, Chem. Rev. 102 (2002) 1897;
J.C.G. Bünzli, N. André, M. Elhabiri, G. Muller, C. Piguet, J. Alloys Compd. 303–304 (2000) 66.
[9] R.L. Carroll, C.B. Gorman, Angew. Chem. Int. Ed. 41 (2002) 4378;
V. Balzani, A. Credi, M. Venturi, Chem. Eur. J. 8 (2002) 5525;
A.H. Flood, J.F. Stoddart, D.W. Steuerman, J.R. Heath, Science 306 (2004) 2055.
[10] V. Balzani, A. Credi, M. Venturi, Molecular Devices and Machines—Concepts and Perspectives for the Nanoworld, Wiley-VCH, Weinheim, Germany, 2007.
[11] J.E. Green, J.W. Choi, A. Boukai, Y. Bunimovich, E. Johnston-Halperin, E. Delonno, Y. Luo, B.A. Sheriff, K. Xu, Y.S. Shin, H.R. Tseng, J.F. Stoddart, J.R. Heath, Nature 445 (2007) 414.
[12] B. Feringa (Ed.), Molecular Switches, Wiley-VCH, Weinheim, 2001;
A.P. de Silva, H.Q.N. Gunaratne, T. Gunnlaugsson, A.J.M. Huxley, C.P. McCoy, J.D. Rademacher, T.E. Rice, Chem. Rev. 97 (1997) 1515.
[13] C. Belle, J.L. Pierre, E. Saint-Aman, New J. Chem. 22 (1998) 1399;
P.R. Ashton, M.C.T. Fyfe, M.V. Martinez-Diaz, S. Menzer, C. Schiavo, J.F. Stoddart, A.J.P. White, D.J. Williams, Chem. Eur. J. 4 (1998) 1523;
L. Fabbrizzi, M. Licchelli, P. Pallavicini, Acc. Chem. Res. 32 (1999) 846;
F.M. Raymo, S. Giordani, A.J.P. White, D.J.J. Williams, Org. Chem. 68 (2003) 4158;
F.M. Raymo, S. Giordani, Org. Lett. 3 (2001) 3475;
Y. Shiraishi, Y. Tokitoh, G. Nishimura, T.A. Hirai, Org. Lett. 7 (2005) 2611.
[14] G.J. Brown, A.P. de Silva, S. Pagliari, Chem. Commun. (2002) 2461;
A.P. de Silva, N.D. McClenaghan, Chem. Eur. J. 10 (2004) 574;
F.M. Raymo, Adv. Mater. 14 (2002) 401;
F.M. Raymo, S. Giordani, Proc. Natl. Acad. Sci. U.S.A. 99 (2002) 4941.
[15] I. Poleschak, J.M. Kern, J.P. Sauvage, Chem. Commun. (2004) 474.
[16] D. Margulies, C.E. Felder, G. Melman, A. Shanzer, J. Am. Chem. Soc. 129 (2007) 347;
D. Margulies, G. Melman, A. Shanzer, J. Am. Chem. Soc. 128 (2006) 4865;
D. Margulies, G. Melman, A. Shanzer, Nat. Mater. 4 (2005) 768;
D. Margulies, G. Melman, C.E. Felder, R. Arad-Yellin, A. Shanzer, J. Am. Chem. Soc. 126 (2004) 15400.
[17] V. Amendola, C. Brusoni, L. Fabbrizzi, C. Mangano, H. Miller, P. Pallavicini, A. Perotti, A. Taglietti, J. Chem. Soc. Dalton Trans. (2001) 3528;
V. Amendola, L. Fabbrizzi, C. Mangano, P. Pallavicini, Struct. Bond. 99 (2001) 79;
V. Amendola, L. Fabbrizzi, P. Pallavicini, Coord. Chem. Rev. 216 (2001) 435;
V. Amendola, L. Fabbrizzi, C. Mangano, P. Pallavicini, Acc. Chem. Res. 34 (2001) 488;
V. Amendola, L. Fabbrizzi, C. Mangano, H. Miller, P. Pallavicini, A. Perotti, A. Taglietti, Angew. Chem. Int. Ed. 41 (2002) 2553.
[18] M. Lieberman, T. Sasaki, J. Am. Chem. Soc. 113 (1991) 1470.
[19] L. Zelikovich, J. Libman, A. Shanzer, Nature 374 (1995) 790.
[20] B.R. Serr, K.A. Andersen, C.M. Elliott, O.P. Anderson, Inorg. Chem. 27 (1988) 4499.
[21] M.T. Youinou, R. Ziessel, J.M. Lehn, Inorg. Chem. 30 (1991) 2144.
[22] N. Fatin-Rouge, S. Blanc, E. Leize, A. Van Dorsselaer, P. Baret, J.L. Pierre, A.M. Albrecht-Gary, Inorg. Chem. 39 (2000) 5771.
[23] R.J.P. Williams, J. Chem. Soc. (1955) 137.
[24] I. Hanazaki, S. Nagakura, Inorg. Chem. 8 (1969) 648.
[25] S. Decurtins, F. Felix, J. Ferguson, H.U. Güdel, A. Ludi, J. Am. Chem. Soc. 102 (1980) 4102.
[26] L. Gil, E. Moraga, S. Bunel, Mol. Phys. 12 (1967) 333.
[27] S.F. Mason, Inorg. Chim. Acta 2 (1968) 89.
[28] P. Hawker, M.V. Twigg, in: G. Wilkinson, R.G. Gillard, J.A. McCleverty (Eds.), Comprehensive Coordination Chemistry, vol. 4, Pergamon Press, Oxford, 1987, p. 1179.
[29] H. Irving, D.H. Mellor, J. Chem. Soc. (1962) 5237.
[30] D. Zurita, P. Baret, J.L. Pierre, New J. Chem. 18 (1994) 1143.
[31] H. Irving, D.H. Mellor, J. Chem. Soc. (1962) 5222.
[32] J.M. Lehn, A. Rigault, J. Siegel, J. Harrowfield, B. Chevrier, D. Moras, Proc. Natl. Acad. Sci. U.S.A. 84 (1987) 2565.
[33] V.A. Grillo, E.J. Seddon, C.M. Grant, G. Aromi, J.C. Bollinger, K. Folting, G. Christou, Chem. Commun. (1997) 1561;
W. Dai, H. Hu, X. Wei, S. Zhu, D. Wang, K. Yu, K. Dalley, X. Kou, Polyhedron 16 (1997) 2059;
C. Piguet, G. Hopfgartner, B. Bocquet, O. Schaad, A.F. Williams, J. Am. Chem. Soc. 116 (1994) 9092.
[34] D.P. Funeriu, Y.B. He, H.J. Bister, J.M. Lehn, Bull. Soc. Chim. Fr. 133 (1996) 673;
B. Kersting, M. Meyer, R.E. Powers, K.N. Raymond, J. Am. Chem. Soc. 118 (1996) 7221.
[35] M. Jaquinod, E. Leize, N. Potier, A.M. Albrecht-Gary, A. Shanzer, A. Van Dorsselaer, Tetrahedron Lett. 34 (1993) 2771;
G. Hopfgartner, C. Piguet, J.D. Henion, J. Am. Soc. Mass Spectrom. (1994) 748.
[36] G. Hopfgartner, C. Piguet, J.D. Henion, A.F. Williams, Helv. Chim. Acta 76 (1993) 1759.
[37] N. Fatin-Rouge, S. Blanc, A. Pfeil, A. Rigault, A.M. Albrecht-Gary, J.M. Lehn, Helv. Chim. Acta 84 (2001) 1694.
[38] H. Gampp, M. Maeder, C.J. Meyer, A.D. Zuberbühler, Talanta 32 (1985) 95.
[39] F.J.C. Rossoti, H.S. Rossoti, R.J. Whewell, J. Inorg. Nucl. Chem. 33 (1971) 2051.
[40] H. Gampp, M. Maeder, C.J. Meyer, A.D. Zuberbühler, Talanta 32 (1985) 257.
[41] H. Gampp, M. Maeder, C.J. Meyer, A.D. Zuberbühler, Talanta 33 (1986) 943.
[42] L.G. Sillen, Acta Chem. Scand. 18 (1964) 1085.
[43] L.G. Sillen, B. Warnqvist, Ark. Kemi. 31 (1968) 377.
[44] J. Havel, Pure Appl. Chem. 34 (1972) 370.
[45] R.A. Palmer, T.S. Piper, Inorg. Chem. 5 (1966) 864.
[46] W.R. McWinnie, J.D. Miller, Adv. Inorg. Chem. Radiochem. 12 (1969) 135.
[47] A. Pfeil, J.-M. Lehn, unpublished results.
[48] A. Rigault, PhD Thesis, Université Louis Pasteur de Strasbourg, France, 1992.
[49] E. Muller, C. Piguet, G. Bernardinelli, A.F. Williams, Inorg. Chem. 27 (1988) 849.
[50] A. Pfeil, J.M. Lehn, J. Chem. Soc. Chem. Commun. (1992) 838.
[51] S. Kitakawa, M. Munakata, A. Hitgashie, Inorg. Chim. Acta 5 (1984) 79.
[52] S. Kitakawa, M. Munakata, A. Hitgashie, Inorg. Chim. Acta 59 (1982) 219.
[53] C.S. Tsai, Can. J. Chem. 45 (1967) 2862.
[54] S. Blanc, P. Yakirevitch, E. Leize, M. Meyer, J. Libman, A. Van Dorsselaer, A.M. Albrecht-Gary, A. Shanzer, J. Am. Chem. Soc. 119 (1997) 4934.
[55] Y. Haas, G. Stein, J. Phys. Chem. 75 (1971) 3668.
[56] G. Blasse, Phys. Stat. Sol. A 130 (1992) K85;
J.C.G. Bünzli, P. Froidevaux, J.M. Harrowfield, Inorg. Chem. 32 (1993) 3306;

S. Petoud, T. Glanzmann, J.C.G. Bünzli, C. Piguet, Q. Xiang, R.P. Thummel, J. Lumin. 82 (1999) 69.
[57] N. Sabbatini, S. Perathoner, V. Balzani, B. Alpha, J.M. Lehn, in: V. Balzani (Ed.), Supramolecular Chemistry, D. Reidel Publishing Co., Dordrecht, 1987.
[58] J.C.G. Bünzli, Lanthanide probes, in: J.C.G. Bünzli, G.R. Choppin (Eds.), Life, Chemical and Earth Sciences: Theory and Practice, Elsevier Science Publ. B.V., Amsterdam, 1989.
[59] A.E. Merbach, E. Tóth (Eds.), The Chemistry of Contrast Agents in Medical Magnetic Resonance Imaging, Wiley, London, 2001.
[60] I. Hemmilä, T. Ståhlberg, P. Mottram, Bioanalytical Applications of Labelling Technologies, Wallac Oy, Turku, 1995;
G. Mathis, in: R. Saez-Puche, P. Caro (Eds.), Rare Earths, Editorial Complutense, Madrid, 1998.
[61] J.-C.G. Bünzli, in: A. Sigel, H. Sigel (Eds.), Metal Ions in Biological Systems, vol. 42, Marcel Dekker Inc., New York, 2004, p. 39.
[62] J.-C.G. Bünzli, Acc. Chem. Res. 39 (2006) 53;
J.C.G. Bünzli, C. Piguet, Chem. Soc. Rev. 34 (2005) 1048.
[63] D.E. Koshland Jr., Angew. Chem. Int. Ed. Engl. 33 (1994) 2375.
[64] C. Piguet, J.C.G. Bünzli, G. Bernardinelli, G. Hopfgartner, A.F. Williams, J. Am. Chem. Soc. 115 (1993) 8197.
[65] R. Tripier, M. Hollenstein, M. Elhabiri, A.S. Chauvin, G. Zucchi, C. Piguet, J.C.G. Bünzli, Helv. Chim. Acta 85 (2002) 1915.
[66] C. Platas Iglesias, M. Elhabiri, M. Hollenstein, J.C.G. Bünzli, C. Piguet, J. Chem. Soc. Dalton Trans. (2000) 2031.
[67] N. Martin, J.C.G. Bünzli, V. McKee, C. Piguet, G. Hopfgartner, Inorg. Chem. 37 (1998) 577.
[68] J. Hamacek, S. Blanc, M. Elhabiri, E. Leize, A. Van Dorsselaer, C. Piguet, A.M. Albrecht-Gary, J. Am. Chem. Soc. 125 (2003) 1541.
[69] M. Elhabiri, R. Scopelliti, J.C.G. Bünzli, C. Piguet, Chem. Commun. (1998) 2347;
M. Elhabiri, R. Scopelliti, J.C.G. Bünzli, C. Piguet, J. Am. Chem. Soc. 121 (1999) 10747.
[70] M. Elhabiri, J. Hamacek, J.C.G. Bünzli, A.M. Albrecht-Gary, Eur. J. Inorg. Chem. (2004) 51.
[71] B. Bernardinelli, C. Piguet, A.F. Williams, Angew. Chem. Int. Ed. Engl. 31 (1992) 1622.
[72] S. Petoud, J.C.G. Bünzli, F. Renaud, C. Piguet, K.J. Schenk, G. Hopfgartner, Inorg. Chem. 36 (1997) 5750.
[73] G. Muller, J.C.G. Bünzli, K.J. Schenk, C. Piguet, G. Hopfgartner, Inorg. Chem. 40 (2001) 2642.
[74] J.F. Desreux, in: J.C.G. Bünzli, G.R. Choppin (Eds.), Lanthanide Probes in Life, Chemical and Earth Sciences: Theory and Practice, Elsevier, Amsterdam, 1989.
[75] J.S. Lindsey, New J. Chem. 15 (1991) 153.
[76] T.M. Garrett, U. Koert, J.M. Lehn, J. Phys. Org. Chem. 5 (1992) 529.
[77] L.J. Charbonnière, A.F. Williams, A. Frey, A.E. Merbach, P. Kamalaprija, O. Schaad, J. Am. Chem. Soc. 119 (1997) 2488.
[78] D. Kalny, M. Elhabiri, T. Moav, A. Vaskevich, I. Rubinstein, A. Shanzer, A.M. Albrecht-Gary, Chem. Commun. (2002) 1426.
[79] A. Budimir, G. Maayan, R. Arad-Yelin, G. Melman, M. Elhabiri, A. Shanzer, A.M. Albrecht-Gary, unpublished results.
[80] S. Abbasi, B. Bhat, R. Sigh, Inorg. Nucl. Chem. Lett. 12 (1976) 391;
B. James, R. Williams, J. Chem. Soc. (1961) 2007;
E. Onstott, H. Laitinen, J. Am. Chem. Soc. 72 (1950) 4724.
[81] R. Nagar, J. Inorg. Biochem. 40 (1990) 349.
[82] A. Odani, H. Masuda, K. Inukai, O. Yamauchi, J. Am. Chem. Soc. 114 (1992) 6294.
[83] K. Sone, J. Am. Chem. Soc. 75 (1953) 5207.
[84] K.P. Balakrishnan, H. Gampp, A.D. Zuberbühler, Helv. Chim. Acta 67 (1984) 2155.
[85] M. Masarwa, H. Cohen, D. Meyerstein, D.L. Hickman, A. Bakac, J.H. Espenson, J. Am. Chem. Soc. 110 (1988) 4293.
[86] D. Goldhaber-Gordon, M.S. Montemerlo, J.C. Love, G.J. Opitec, J.C. Ellenbogen, Proc. IEEE 85 (1997) 1.
[87] C. Canevet, J. Libman, A. Shanzer, Angew. Chem. Int. Ed. Engl. 35 (1996) 2657.
[88] A.M. Albrecht-Gary, S. Blanc, N. Fatin-Rouge, J. Libman, A. Shanzer, L. Zelikovich, unpublished results.
[89] N. Fatin-Rouge, Thesis, Université Louis Pasteur, France, 1998.
[90] J.P. Collin, P. Gaviña, J.P. Sauvage, New J. Chem. 21 (1997) 525.
[91] A. Livoreil, J.P. Sauvage, N. Armaroli, V. Balzani, L. Flamigni, B. Ventura, J. Am. Chem. Soc. 119 (1997) 12114.
[92] L. Raehm, J.M. Kern, J.P. Sauvage, Chem. Eur. J. 5 (1999) 3310.
[93] J.P. Collin, F. Durola, P. Mobian, J.P. Sauvage, Eur. J. Inorg. Chem. (2007) 2420.
[94] B.R. James, R.J.P. Williams, J. Chem. Soc. (1961) 2007.
[95] D.J. Cárdenas, A. Livoreil, J.P. Sauvage, J. Am. Chem. Soc. 118 (1996) 11980.
[96] R.G. Wilkins, Kinetics and Mechanism of Reactions of Transition Metal Complexes, VCH Publishers, Weinheim, 1991.
[97] A. Petitjean, N. Kyritsakas, J.M. Lehn, Chem. Eur. J. 11 (2005) 6818.
[98] R. Kikkeri, H. Traboulsi, N. Humbert, E. Gumienna-Kontecka, R. Arad-Yellin, G. Melman, M. Elhabiri, A.M. Albrecht-Gary, A. Shanzer, Inorg. Chem. 46 (2007) 2485.
[99] A. Corsini, R.M. Cassidy, Talanta 26 (1978) 297.
[100] W.R. Harris, C.J. Carrano, K.N. Raymond, J. Am. Chem. Soc. 101 (1979) 2213.
[101] S. Cabani, M. Landucci, E. Scrotto, J. Chem. Soc. (1962) 88;
S. Cabani, M. Landucci, J. Chem. Soc. (1962) 278;
S. Musso, G. Anderegg, H. Ruegger, Inorg. Chem. 34 (1995) 3329;
G. Atkinson, J. Bauman, Inorg. Chem. 1 (1962) 900;
R. Grieser, H. Sigel, Inorg. Chem. 10 (1971) 2229.
[102] T.Y. Matrosovich, F.I. Lobanov, N.V. Mahanov, Zh. Neorg. Khim. 31 (1986) 1441.
[103] E. Bardez, I. Devol, B. Larrey, B. Valeur, J. Phys. Chem. B 101 (1997) 7786;
F. Launay, V. Alain, E. Destandau, N. Ramos, E. Bardez, P. Baret, J.L. Pierre, New J. Chem. 25 (2001) 1269.
[104] F. Quentel, J.Y. Carbon, M. L'Her, J. Courtot-Coupez, Anal. Chim. Acta 96 (1978) 133;
B.W. Budesinsky, Anal. Chem. 47 (1975) 560;
R. Nasanen, U. Penttinen, Acta Chem. Scand. 6 (1952) 837.